Supporting information

Regulating the bubble-water/catalyst interface microenvironment for accelerated electrosynthesis H_2O_2 via optimizing oxygen functional groups on carbon black

Yuanyuan Zhang,‡[a] Xuan Zheng,‡[a] Hui Su,[a] Yun Ling,*[a,b] Rong Guo,[a] Maosheng Zhang,[a] Qingxiang Wang,*[a] and Li Niu*[c]

[a]*Fujian Provincial Key Laboratory of Modern Analytical Science and Separation Technology, Fujian Provincial Key Laboratory of Pollution Monitoring and Control, College of Chemistry, Chemical Engineering and Environment, Minnan Normal University, Zhangzhou, 363000, China*

[b]*Key Laboratory of Advanced Energy Materials Chemistry (Ministry of Education), Nankai University, Tianjin, 300071, China*

[c]*Guangdong Engineering Technology Research Center for Photoelectric Sensing Materials & Devices, Guangzhou Key Laboratory of Sensing Materials & Devices, Center for Advanced Analytical Science, School of Chemistry and Chemical Engineering, Guangzhou University, Guangzhou 510006, China*

*Corresponding Authors.

E-mail addresses: lingyun@mnnu.edu.cn (Y. Ling), axiang236@vip.163.com (Q. Wang), lniu@gzhu.edu.cn (L. Niu)

‡ These authors contributed equally to this work.

1. Experimental sections

1.1. Chemicals

Cabot Vulcan XC-72 Carbon Black and Cerium sulfate tetrahydrate were purchased from Shanghai Macklin Biochemical Technology Co., Ltd. Potassium hydroxide was supplied by Sinopharm Chemical Reagent Co., Ltd., and ethyl alcohol was purchased from Xilong Scientific Co., Ltd. Nafion solution was sourced from DuPont, and carbon paper (CP, TGP-H-060) was acquired from Toray Industries, Japan. O_2 and Ar gas (99.999%) were purchased from Zhangzhou Haolilai Gas Co., Ltd. All solutions were prepared using deionized water with a resistivity greater than 18.2 MΩ·cm, obtained from a Kertone Lab Day-20 system.

1.2. Electrochemical Measurement

All potentials in this system were calibrated to the reversible hydrogen electrode (RHE) scale using the following equation:

$$E\,(\text{V vs. RHE}) = E\,(\text{V vs. Hg/HgO}) + 0.059\,\text{pH} + 0.098 \quad (1)$$

The selectivity of H_2O_2 (H_2O_2%) and the number of transferred electrons (n) were calculated using the disk current (I_{disk}) and ring current (I_{ring}) based on the following equations[1,2]:

$$H_2O_2(\%) = 200 \times \frac{I_{ring}/Nc}{(I_{ring}/Nc) + |I_{disk}|} \quad (3)$$

$$n = 4 \times \frac{|I_{disk}|}{(I_{ring}/Nc) + |I_{disk}|}$$

Where I_{disk} is the disk current and I_{ring} is the ring current. In addition to the RRDE method described above, the n can also be determined using the disk current density obtained from the rotating disk electrode (RDE) measurements. The RDE used has a geometric disk area of 0.196 cm^2.

To perform the Koutecky-Levich (K-L) analysis, the RDE experiments were conducted at electrode rotation speeds of 400, 625, 900, 1225, 1600, and 2025 rpm. The K-L equation was used to calculate the electron transfer number (n) as follows [3,4]:

$$\frac{1}{j} = \frac{1}{j_k} + \frac{1}{B\omega^{1/2}} \quad (4)$$

$$B = 0.62 \times n \times F \times C_{O_2} \times D_{O_2}^{2/3} \times v^{-1/6} \quad (5)$$

Where j and j_k are the current density and dynamic current density (mA cm^{-2}) respectively, ω is the angular velocity (rpm), F is the Faraday constant (96485 C mol^{-1}), C_{O_2} is the O_2 concentration (1.2×10^{-6} mol cm^{-3}), D_{O_2} represents the diffusion coefficient of O_2 (1.9×10^{-5} cm^2 s^{-1}), v defines the kinematic viscosity of O_2 (1×10^{-2} cm^2 s^{-1}).

The selectivity of H_2O_2 in the ORR process[5,6] is calculated by the following equation:

$$H_2O_2\% = \left(2 - \frac{n}{2}\right) \times 100$$

1.3. Methylene blue degradation experiment

Prior to the experiment, a methylene blue (MB) solution with a concentration of 10

mg L^{-1} was prepared, and a calibration curve correlating absorbance to MB concentration was established using UV-vis spectrophotometry. The catalyst CB-85-6h, with a loading of 0.1 mg cm^{-2}, was employed as the working electrode in an H-type electrolytic cell. Following electrolysis at a constant potential of 0.2 V vs. RHE, 2 mL of the cathode electrolyte was collected and acidified with 0.5 M H_2SO_4 containing 1 mM Fe^{2+} to generate a strong oxidizing agent. Subsequently, 5 mL of the standard MB solution (10 mg L^{-1}) was rapidly added to the oxidized solution, followed by gentle mixing. The residual concentration of MB after degradation was calculated using the following equation:

2. Additional figures and table

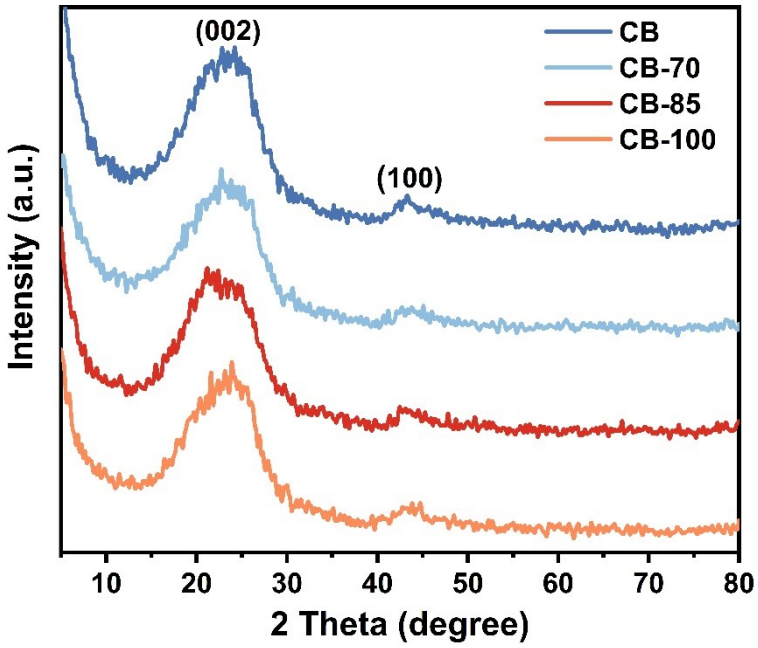

Fig. S1. XRD patterns of CB treated at different temperatures.

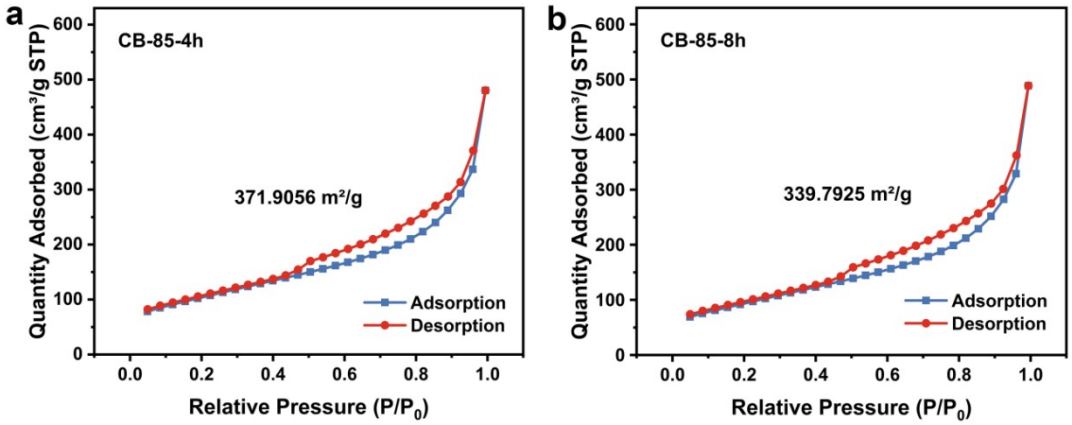

Fig. S2. BET adsorption-desorption isotherms of CB-85-4h (a) and CB-85-8h (b).

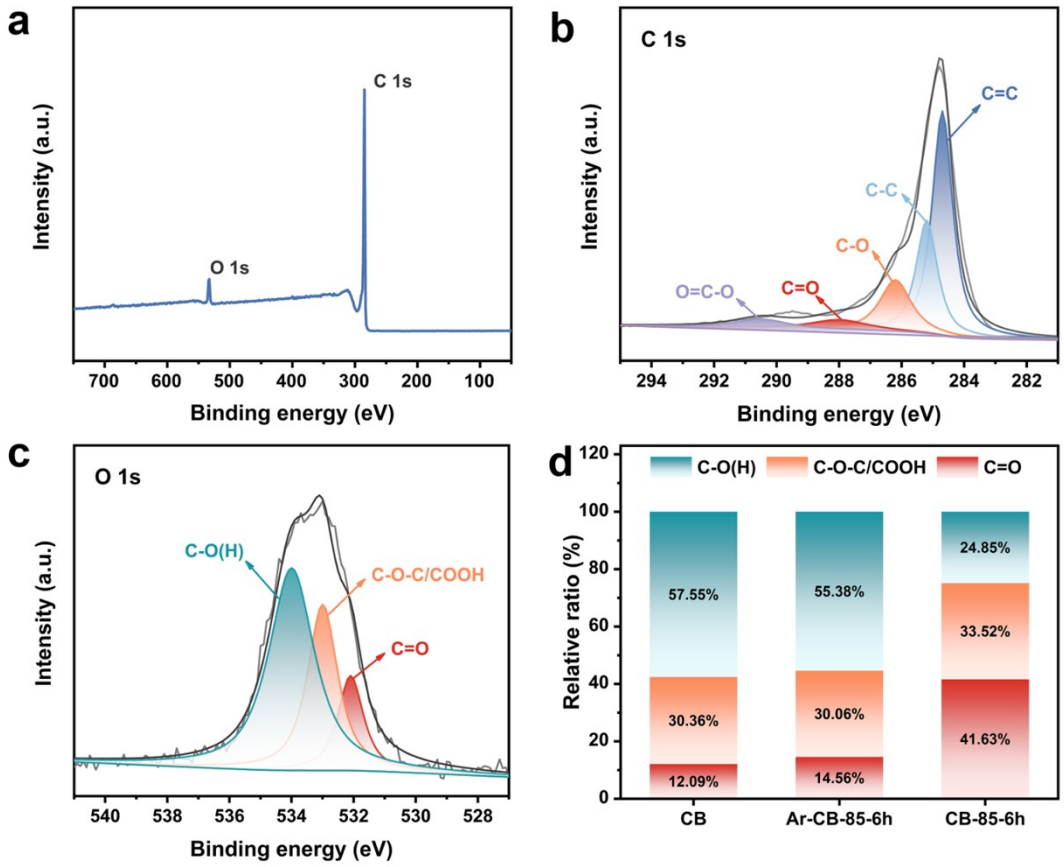

Fig. S3. (a) XPS full spectra of Ar-CB-85-6h. High-resolution XPS spectra of (b) C 1*s* and (c) O 1*s* of Ar-CB-85-6h. (d) The relative ratio of oxygen functional groups in Ar-CB-85-6h.

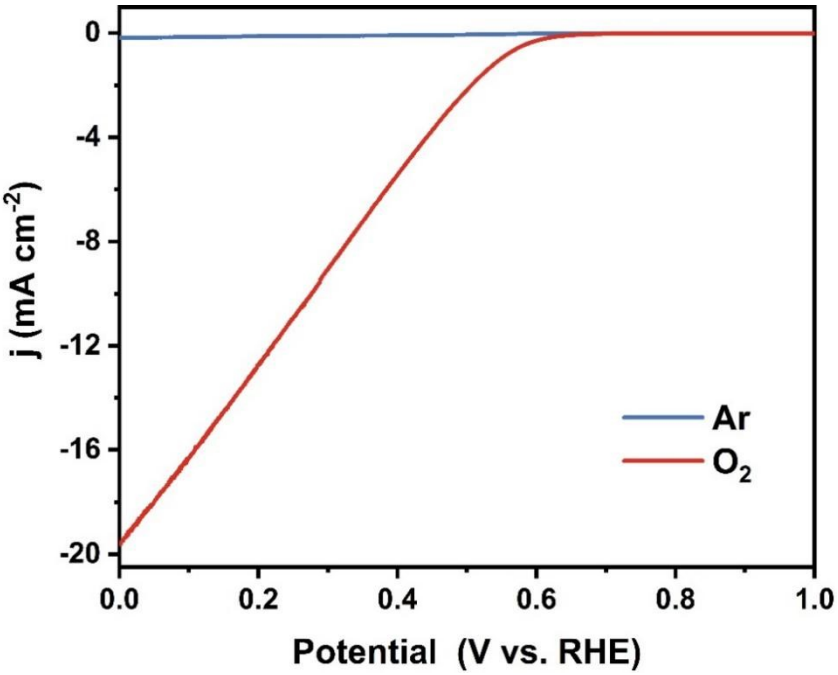

Fig. S4. LSV curves of CB-85-6h in Ar- and O_2-saturated 0.1 M KOH solution with a scan rate of 5 mV s^{-1}.

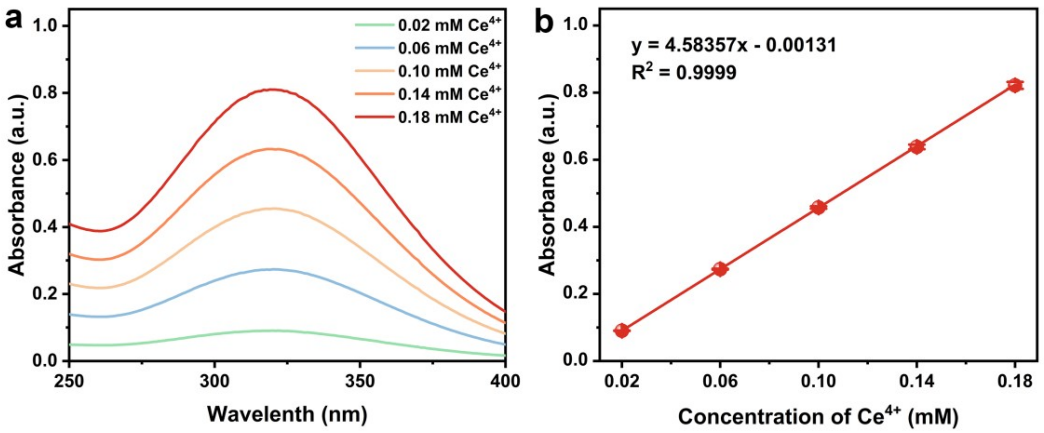

Fig. S5. (a) UV-vis spectra of Ce^{4+} solutions with different concentrations. (b) Linear calibration curve between Ce^{4+} concentration and absorbance.

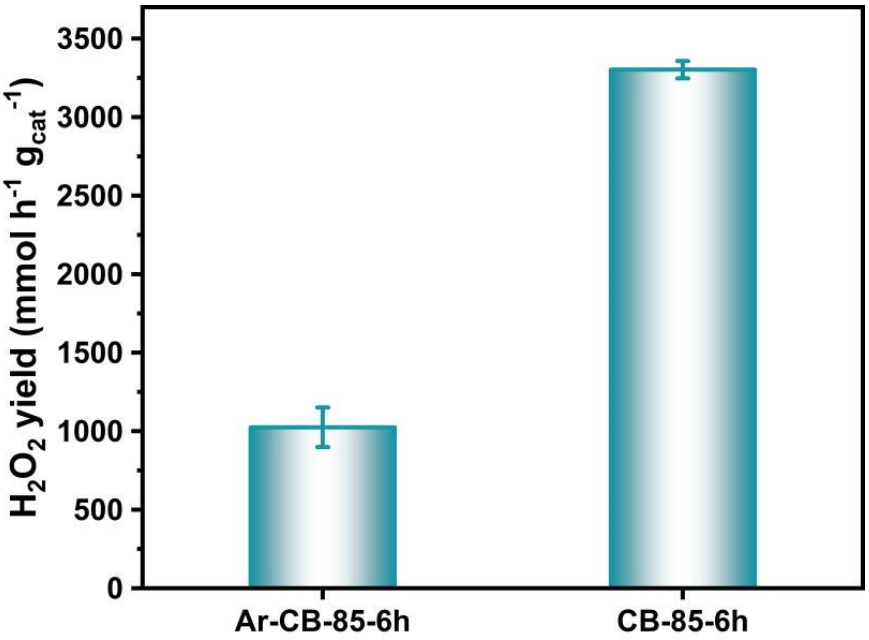

Fig. S6. Comparison of H_2O_2 yield between Ar-CB-85-6h and CB-85-6h at 0.2 V vs. RHE.

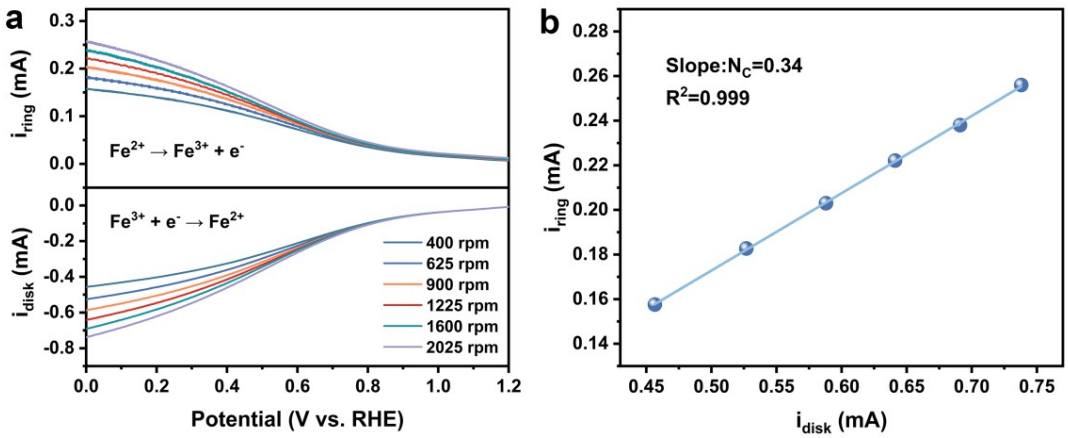

Fig. S7. RRDE collection efficiency calibration. (a) LSV curves tested in N_2 saturated 0.1 M KOH electrolyte containing 10 mM $K_3Fe(CN)_6$ (scan rate: 20 mV s^{-1}, E_{ring}: 1.55 V vs. RHE). (b) Linear fitting of diffusion-limited current density recorded on a ring electrode at different speeds (the collection efficiency is the ratio of the absolute value of the ring current to the disk current).

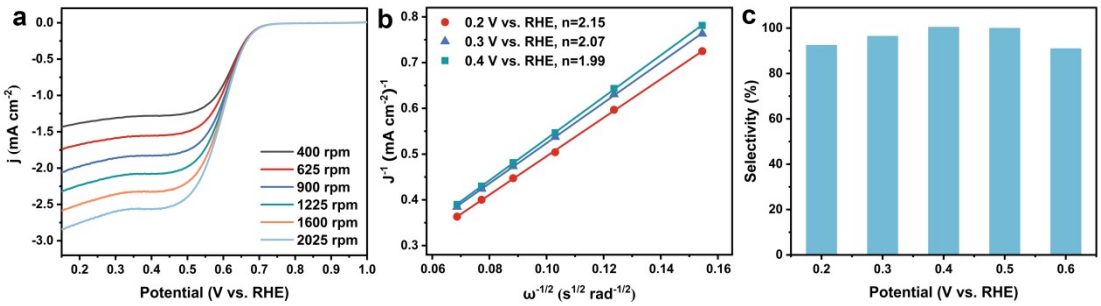

Fig. S8. (a) LSV curves of CB-85-6h with 10 mV s^{-1} at different rotating speed. (b) K-L plots of CB-85-6h at different potentials. (c) Selectivity of H_2O_2 at different potentials for CB-85-6h.

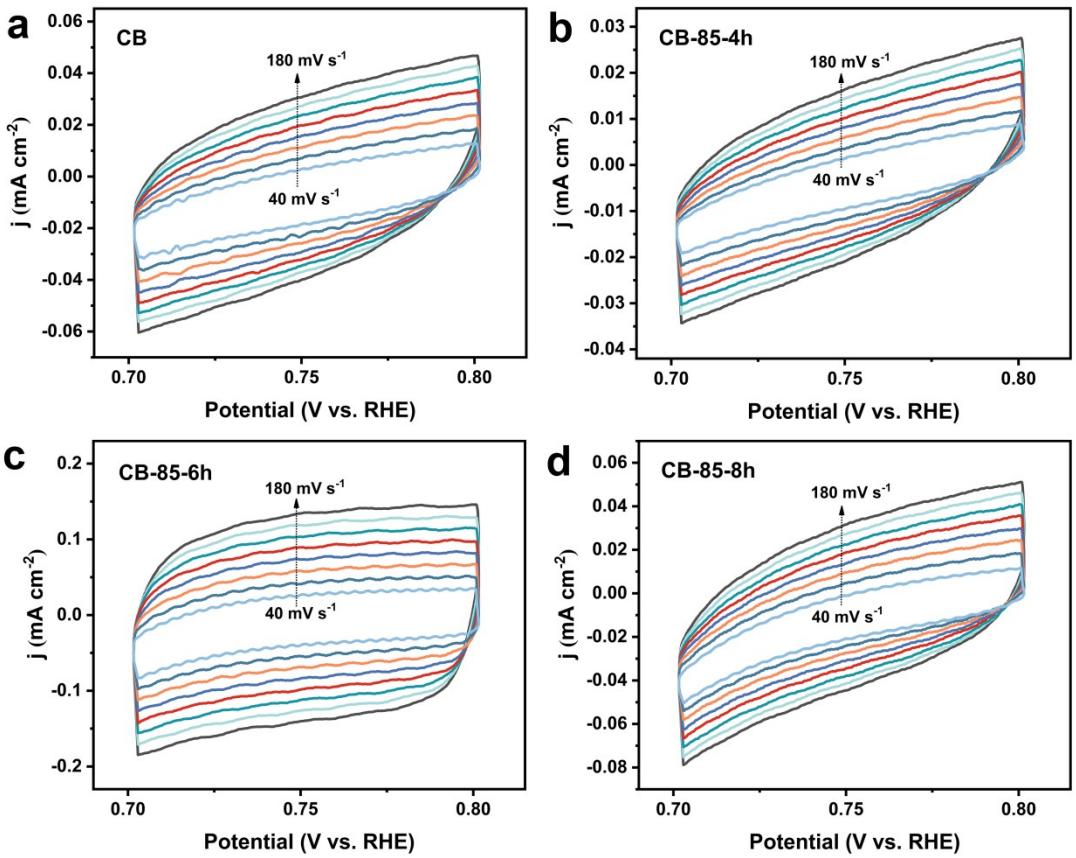

Fig. S9. CV curves of CB (a), CB-85-4h (b), CB-85-6h (c) and CB-85-8h (d) in 0.1 M KOH solution at different scanning rates.

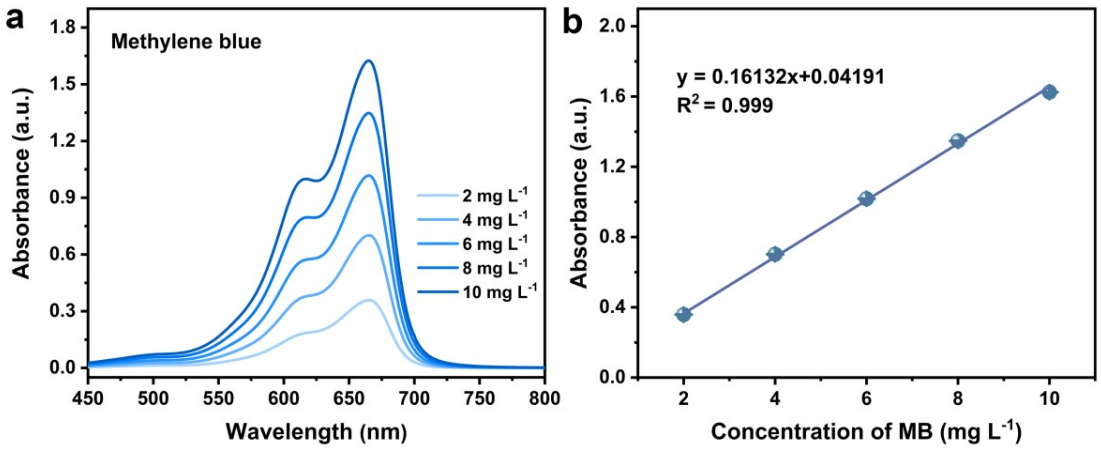

Fig. S10. (a) UV-vis spectra of MB solutions with different concentrations. (b) Linear relationship between MB concentration and absorbance.

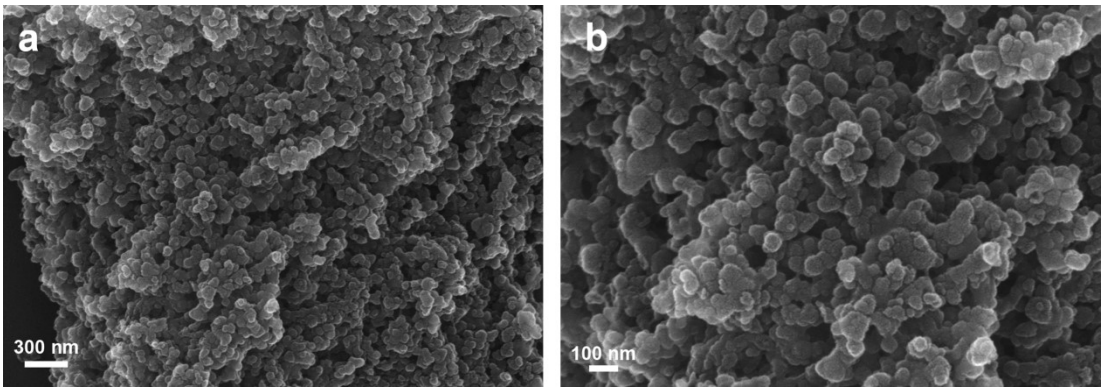

Fig. S11. SEM images of CB-85-6h catalyst after electrochemical test.

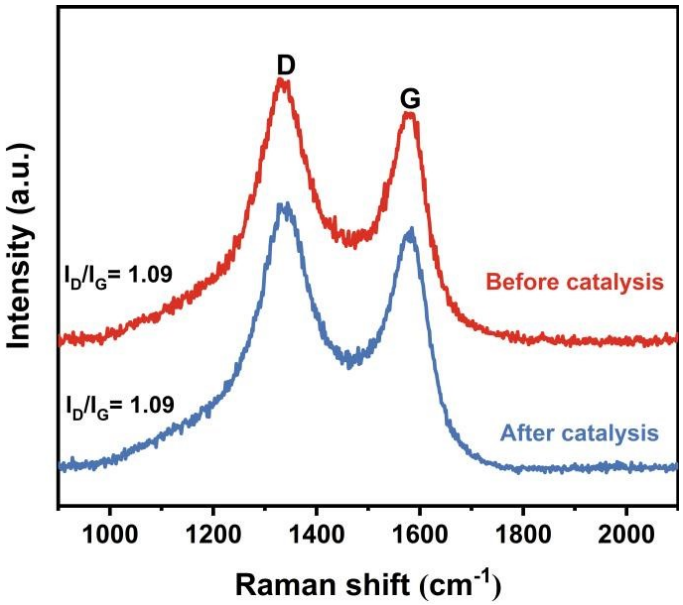

Fig. S12. Raman spectra of CB-85-6h catalyst before and after electrochemical test.

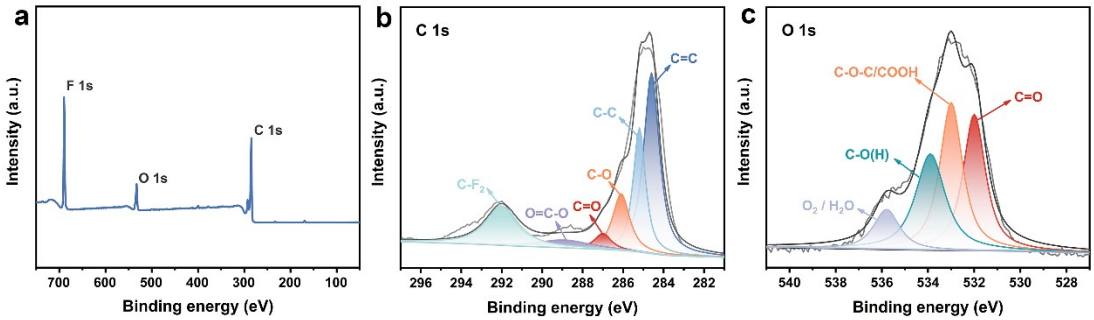

Fig. S13. XPS full spectra of d CB-85-6h (a), high-resolution XPS spectra of C 1*s* (b) and O 1*s* (c) after electrochemical test.

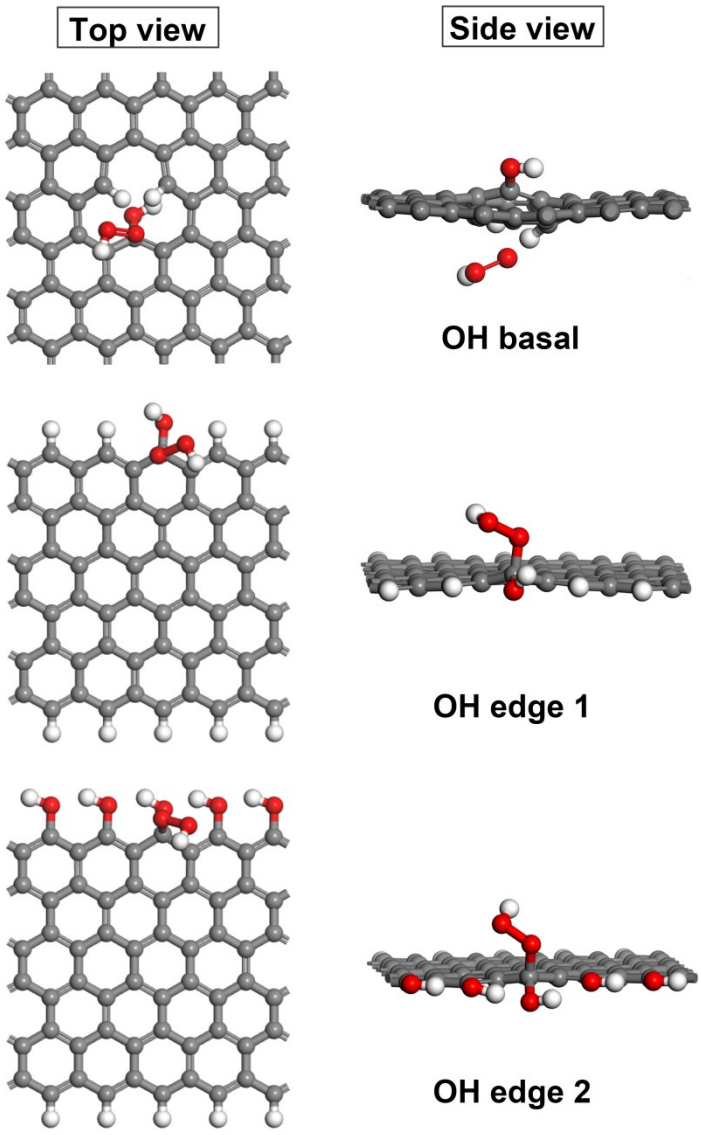

Fig. S14. Top and side view of *OOH adsorption configuration on hydroxy-doped carbon surface.

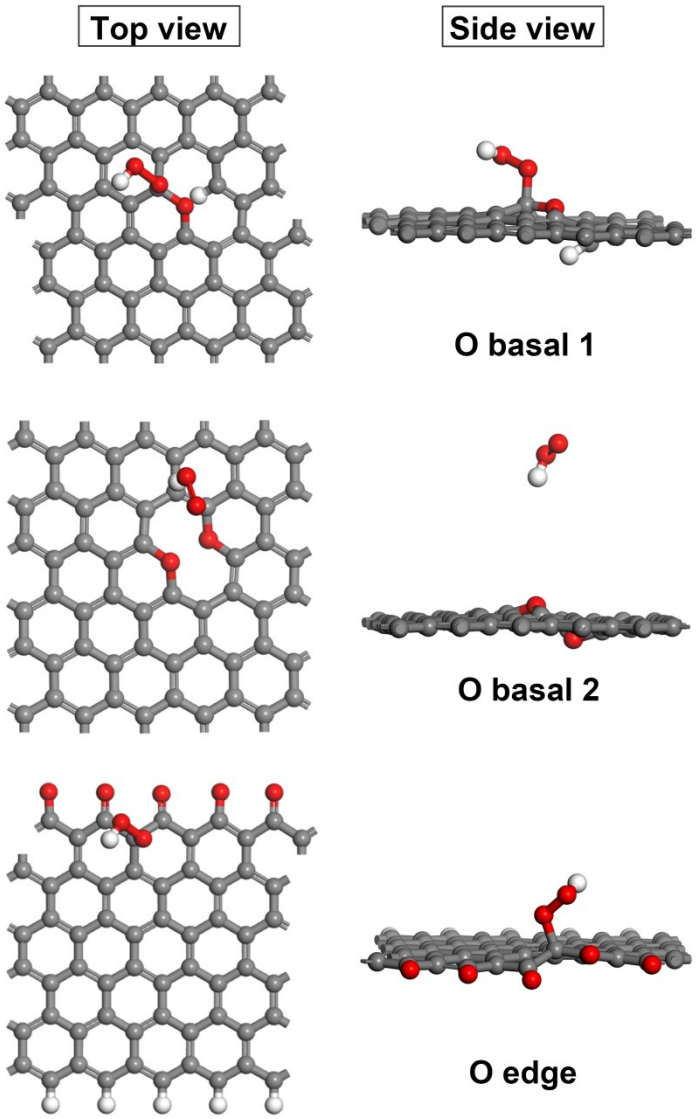

Fig. S15. Top and side views of *OOH adsorption configurations on ether- and carbonyl-doped carbon surfaces.

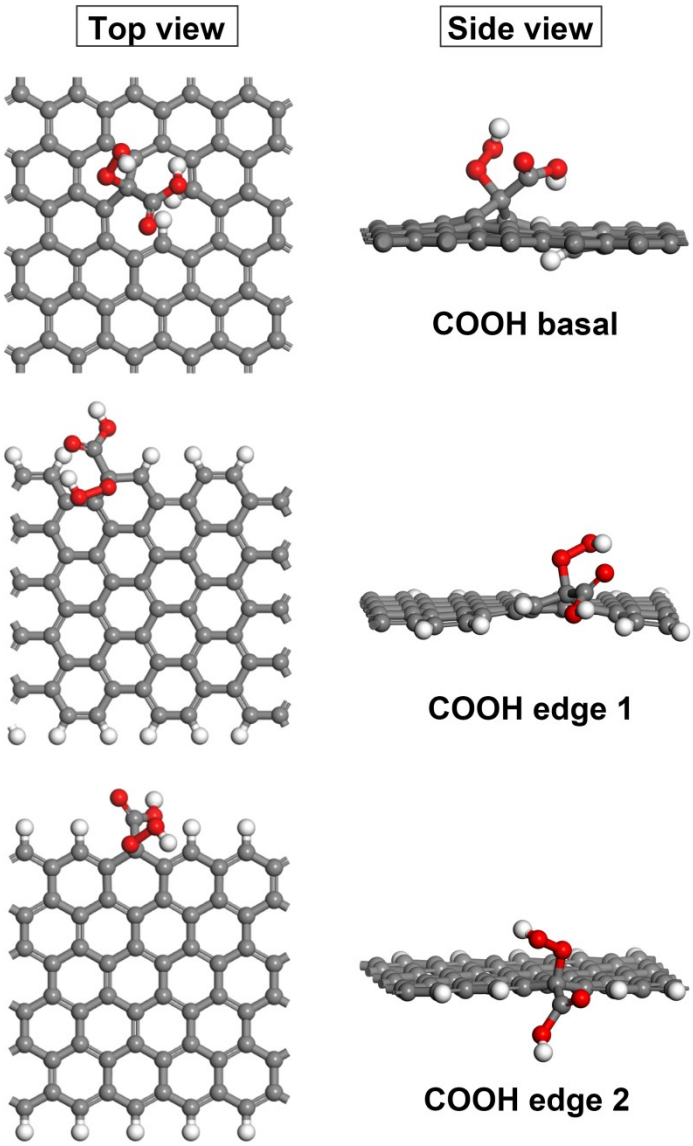

Fig. S16. Top and side view of *OOH adsorption configuration on carboxyl-doped carbon surface

Table S1. Comparison of CB-85-6h catalyst for H_2O_2 production with other catalysts reported in recent literature.

Catalysts	Electrolyte	Potential	Production rate	Ref.
CB-85-6h	**0.1 M KOH**	**0.20**	**3302.23 mmol h^{-1} g_{cat}^{-1}**	**This work**
H-CNT	0.1 M KOH	0.70	748 mmol h^{-1} g_{cat}^{-1}	7
N,O-CNTs	1 M KOH	0.15	264.8 mmol h^{-1} g_{cat}^{-1}	8
er-VG-vacuum	0.1 M KOH	0.40	1767 mmol h^{-1} g_{cat}^{-1}	9
Mo-CDC-30	0.1 M KOH	0.55	455 mmol h^{-1} g_{cat}^{-1}	10
OCNTs-6	0.1 M KOH	0.40	296.84 mmol h^{-1} g_{cat}^{-1}	11
Co_{SA}-N-CNTs	0.5 M H_2SO_4	0.00	974 mmol h^{-1} g_{cat}^{-1}	12
Mn-TiO_2	0.1 M KOH	0.78	1810 mmol h^{-1} g_{cat}^{-1}	13
CuSn400	0.1 M KOH	0.10	1436 mmol h^{-1} g_{cat}^{-1}	14

Table S2. DFT results of the Gibbs adsorption free energy (ΔG), limiting potential (U_L), and overpotential (η) of *OOH involved in ORR on graphene surfaces functionalized with different oxygen groups

Structure	ΔG_{*OOH}/eV	U_L/V	η/V
COOH edge 1	4.13	0.61	0.094
OH basal	3.45	-0.07	0.770
O basal 1	2.96	-0.56	1.262
COOH basal	3.20	-0.32	1.017
O basal 2	3.72	0.20	0.504
COOH edge 2	2.31	-1.21	1.908
OH edge 2	2.53	-0.99	1.694
O edge 2	3.65	0.13	0.574
OH edge 1	2.29	-1.23	1.928

References

1 R. Xie, C. Cheng, R. Wang, J. Li, E. Zhao, Y. Zhao, Y. Liu, J. Guo, P. Yin and T. Ling, *ACS Catal*., 2024, **14**, 4471-4477.
2 S. Xue, X. Li, Y. Sun, W. Cui, F. Cao, Z. Cao, Y. Huang, M. Shao, Z. Li and L. Zhi, *Angew. Chem. Int. Ed.*, 2024, 202420063.
3 F. Sun, C. Yang, Z. Qu, W. Zhou, Y. Ding, J. Gao, G. Zhao, D. Xing and Y. Lu, *Appl. Catal. B*, 2021, **286**, 119860.
4 Y. J. Sa, J. H. Kim and S. H. Joo, *Angew. Chem. Int. Ed.*, 2019, **58**, 1100-1105.
5 J. Park, Y. Nabae, T. Hayakawa and M. a. Kakimoto, *ACS Catal.*, 2014, **4**, 3749-3754.
6 Q. Zhao, J. An, S. Wang, Y. Qiao, C. Liao, C. Wang, X. Wang and N. Li, *ACS Appl. Mater. Interfaces*, 2019, **11**, 35410-35419.
7 S. Hu, Y. Zhan, P. Wang, J. Yang, F. Wu, M. Dan and Z. Q. Liu, *Chem. Eng. J.*, 2023, **465**, 142906.
8 S. Xu, R. Lu, K. Sun, J. Tang, Y. Cen, L. Luo, Z. Wang, S. Tian and X. Sun, *Adv. Sci.*, 2022, **9**, 2201421.
9 D. Zhang, C. Tsounis, Z. Ma, D. Djaidiguna, N. M. Bedford, L. Thomsen, X. Lu, D. Chu, R. Amal and Z. Han, *Small*, 2021, **18**, 2105082.
10 C. Zhang, C. Wu, L. Wang and G. Liu, *ACS Appl. Mater. Interfaces*, 2023, **15**, 838-847.
11 W. Liu, C. Li, G. Ding, G. Duan, Y. Jiang and Y. Lu, *J. Materiomics*, 2022, **8**, 136-143.
12 W. Liu, C. Zhang, J. Zhang, X. Huang, M. Song, J. Li, F. He, H. Yang, J. Zhang and D. Wang, *Appl. Catal. B*, 2022, **310**, 121312.
13 Q. Chen, S. Yan, J. Liang, K. Dong, Y. Luo, Q. Liu, T. Li, Y. Wang, L. Yue, B. Zheng, Y. Liu, S. Gao, Z. Jiang, W. Li and X. Sun, *ACS Appl. Mater. Interfaces*, 2021, **13**, 46659−46664.
14 L. Liu, C. Yan, X. Luo, C. Li, D. Zhang, H. Peng, H. Wang, B. Zheng and Y. Guo, *Inorg. Chem. Front.*, 2023, **10**, 3632-3640.